Geotech Geol Eng (2024) 42:2299–2320
https://doi.org/10.1007/s10706-023-02673-5

ORIGINAL PAPER

Elastic–Plastic Analysis of Rigid Passive Piles in Two-Layered Soils

Ivo Bellezza

Received: 6 July 2020 / Accepted: 30 September 2023 / Published online: 21 December 2023

Abstract The paper analyses the behavior of a rigid passive pile embedded in a soil profile consisting of a stable layer underlying an unstable layer subjected to a uniform soil displacement. Pile-soil interaction is considered by modeling the soil by a series of elastic–plastic springs along the pile shaft. The modulus of horizontal subgrade reaction is assumed to linearly increase with depth in the unstable layer and constant in the stable one. The ultimate soil resistance is assumed increasing with depth in both layers. The results of analysis are presented in dimensionless form in terms of shear force developed at the slip surface as a function of the pile embedment into the stable layer and the distribution of soil characteristics over depth. The method allows capturing pile response not only at the soil ultimate state but also at the intermediate states. Specifically, the governing equations for the elastic, elastic–plastic and plastic cases are discussed and, whenever possible, a set of closed-form expressions is provided to estimate the maximum bending moment along the shaft and the pile head deflection, so that for an assigned value of the required stabilizing force both ultimate and serviceability limit state of the pile can be checked. A numerical example is given to illustrate the application of the proposed procedure.

I. Bellezza (✉)
Department S.I.M.A.U., Università Politecnica delle Marche, Via Brecce Bianche, 60121 Ancona, Italy
e-mail: i.bellezza@staff.univpm.it

Keywords Limit equilibrium methods · Slope stability · Non-linear response · Lateral loading · Piles · Closed-form solutions · Soil movement · Soil–structure interaction

List of Symbols

$A, B; C, \Delta, X, Y$	Auxiliary functions of λ, R_U and ρ
b	Depth of negative soil plasticization in the unstable soil; $b_n = b/L_1$
c	Depth of positive soil plasticization in the unstable soil; $c_n = c/L_1$
D	Pile diameter
E_P	Young's modulus of pile
E_{S1} (E_{S2})	Modulus of subgrade reaction in the unstable (stable) layer
f	Final depth of negative soil plasticization in the stable soil; $f_n = f/L_1$
f_{Tys}, f_{yT}, f_{MT}	Functions of λ and R_E
g	Initial depth of positive soil plasticization in the stable soil; $g_n = g/L_1$
J_P	Moment of inertia of pile
L	Pile length ($=L_1+L_2$); L_n = normalized pile length = $L/L_1 = 1+\lambda$
L_1 (L_2)	Pile length in the unstable (stable) layer
m_1 (m_2)	Gradient of P_u in the unstable (stable) layer
$M(z)$	Bending moment at depth z; $M_n = M/m_1$L

M_{max}	Maximum bending moment; M_{maxn} = normalized bending moment $(=M_{max}/(m_1L_1^3))$
n	Gradient of E_{S1} in the unstable layer
P_e	Soil reaction per unit length in elastic conditions
P_{u1} (P_{u2})	Ultimate force per unit length in the unstable (stable) layer
R_E	Subgrade modulus ratio at the layer interface = $E_{S2}/(nL_1)$
R_U	Strength ratio at the layer interface = $P_{u20}/(m_1L_1)$
$T(z)$	Shear force at depth z; $T_n = T/m_1L_1^2$
T_s	Shear force at the sliding depth $z = L_1$; $T_{sn} = T_s/(m_1L_1^2)$
T_{sne}	T_{sn} at the elastic threshold
T_{snp}	T_{sn} at the plastic threshold
T_{snR}	T_{sn} requested to stabilize a slope
y_0	Pile head deflection; y_{0n} = normalized pile head deflection = $y_0\ E_{s2}/m_1L_1$
$y_p(z)$	Pile deflection at depth z
y_s	Soil movement; y_{sn} = normalized soil movement = $y_s\ E_{s2}/m_1L_1$
y_{s0}	Soil movement at z = 0; y_{s0n} = normalized soil movement at z = 0 = $y_{s0}\ E_{s2}/m_1L_1$
y_{s0nA}	Normalized limiting soil movement relevant to first soil plasticization above the sliding surface
y_{s0nB}	Normalized limiting soil movement relevant to first soil plasticization below the sliding surface
y_{s0nH}	Normalized limiting soil movement relevant to first soil plasticization at the pile head
y_{s0ne}	Normalized soil movement at the elastic threshold
y_{s0np}	Normalized soil movement at the plastic threshold
z	Generic depth; $z_n = z/L_1$
z_{m1} (z_{m2})	Depth of maximum bending moment above (below) the sliding surface; $z_{m1n} = z_{m1}/L_1$; $z_{m2n} = z_{m2}/L_1$
λ	Embedment ratio = L_2/L_1
ω	Rotation angle of rigid pile; ω_n = normalised rotation angle = $\tan\omega\ E_{s2}/m_1$
ρ	$m_2 : m_1$

1 Introduction

Slope stability is often improved by using passive piles. In recent decades there have been several reports in the literature on successful use of piles to stabilize a slope (e.g. Sommer 1977; Fukuoka 1977; Reese et al. 1992; Poulos 1995; Smethrust and Powrie 2007).

Different methods have been proposed to evaluate the performance and design of reinforcing piles in slopes, as well as to evaluate the safety factor of a reinforced slope (Ito et al. 1979, 1981, 1982; Chow 1996, Hassiotis et al. 1997, Cai and Ugai 2000, 2011; Ausilio et al. 2001; Jeong et al. 2003, Won et al. 2005, Wei and Cheng 2009, Ellis et al. 2010, Yamin and Liang 2010; Kourkoulis et al. 2011, 2012; Ashour and Ardalan 2012; Galli et al. 2017; Di Laora and Fioravante 2018). However a widely accepted design procedure is still lacking (Di Laora et al. 2017). As an example, the effect of stabilizing piles on slope stability is considered somewhere as an additional resistance (e.g. Poulos 1995) and elsewhere as a negative action (e.g.Yamin and Liang 2010). Moreover a clear distinction should be made between piles installed to arrest an active landslide and piles used as a preventive measure in stable slopes. In the former case the pile design can be reasonably based on the assumption that the critical slip surface, on which residual strength is mobilized, does not change after the pile installation. In the latter case the pile response must be evaluated for different locations of the potential slip surface and it is likely that the critical slip surface varies respect to the unreinforced slope (Hassiotis et al. 1997).

Although numerical three-dimensional analyses are in principle the most rigorous approach to analyze the problem, they are computationally intensive and time-consuming. Therefore in the practice the so-called decoupled methods are widely used, in which the behavior of slope and piles is analyzed separately (Viggiani 1981; Poulos 1995). This design approach may be simplified in three main steps: (a) computing the lateral force needed to increase the factor of safety of the slope to the target value using the traditional limit equilibrium methods; (b) evaluating the shear force that each pile can offer as a consequence of soil sliding; (c) selecting a pile configuration able to provide this required force without structural damage. The available approaches in the literature (Viggiani 1981; Di Laora et al. 2017; Bellezza and Caferri 2018) are mainly based on the assumption that soil strength is fully mobilized along the Soil–pile interface and, at varying the depth of sliding respect to pile length, a set of analytical expressions is provided for the shear and moment which have to be included in the computation of the safety factor of the reinforced slope (Lee et al. 1995). These procedures refer to the ultimate state only, giving no indication on pile response at intermediate states prior to the ultimate state and on pile and soil movement required to achieve the ultimate state. Alternatively, some analytical methods assume a soil response fully elastic (e.g. Chen and Poulos 1997; Cai and Ugai 2003, 2011; Guo 2014) whereas the elastic–plastic condition is rarely investigated. To overcome these drawbacks, Poulos (1995) proposed a valuable displacement-based design procedure for a passive pile embedded on a continuum elastic, but even for simplified soil profiles the solution is not given in closed-form and the application to real cases requires the use of a specific computer program.

Nowadays the general trend in engineering practice is to install stabilizing piles with a center to center spacing of three/four pile diameter which is the most effective solution to assure the development of soil arching (Ellis et al. 2010). To increase the structural capacity, the use of large pile diameters with a high reinforcement ratio is recommended (Kourkoulis et al. 2011). Therefore, in certain circumstances, the assumption of rigid deformation for the pile can be reasonable.

Bellezza et al. (2017) presented an example of elastic–plastic analysis of rigid passive piles embedded in a single layer with modulus of subgrade reaction and strength linearly increasing with depth providing design charts for pile displacement and maximum bending moment at varying the shear force at the sliding surface. More recently, Lei et al. (2022) proposed an analysis for flexible piles embedded in cohesive layered soils assuming both strength and modulus of subgrade reaction constant with depth.

In this paper a similar analysis is extended to a more realistic two-layer soil profile with soil strength linearly increasing with depth in both layers. The purpose of this study is to provide an effective tool to analyze the pile response at varying the soil movement, so that the pile contribution in terms of stability can be evaluated not only at the ultimate state but also at intermediate states.

2 Method of Analyis

Figure 1 shows a passive pile of length L and diameter D embedded for a length L_1 a layer subjected to a lateral soil movement y_s and for a length L_2 in a stable layer.

The rigid displacement of the pile, y_p, at any depth z can be written as

$$y_p = y_0 - \tan\omega \cdot z \tag{1}$$

where y_0 is the pile head displacement and ω is the rotation angle.

Similarly to previous studies (e.g. Hassiotis et al. 1997; Cai and Ugai 2000; Gou 2014) the elastic soil reaction [FL^{-1}] is calculated by modeling the soil as a series of independent springs:

$$P_e = -E_s\left(y_p - y_s\right) \tag{2}$$

where E_s is the modulus of subgrade reaction [FL^{-2}].

According to Poulos (1995) a uniform distribution of soil movement is assumed in the unstable layer:

$$y_s = \begin{cases} y_{s0} & 0 \le z \le L_1 \\ 0 & L_1 < z \le L \end{cases} \tag{3}$$

In the unstable layer the modulus of horizontal subgrade reaction E_{S1} and the ultimate lateral soil resistance P_{u1} [FL^{-1}] vary linearly with depth:

$$E_{S1} = n \cdot z \tag{4}$$

$$P_{u1} = m_1 \cdot z \tag{5}$$

where n [FL^{-3}] and m_1 [FL^{-2}] are the gradient of E_s and P_{u1}, respectively.

In the stable layer the horizontal subgrade reaction is assumed to be constant (E_{S2}), whereas the ultimate soil strength is assumed to linearly increase with depth (Fig. 1d–e):

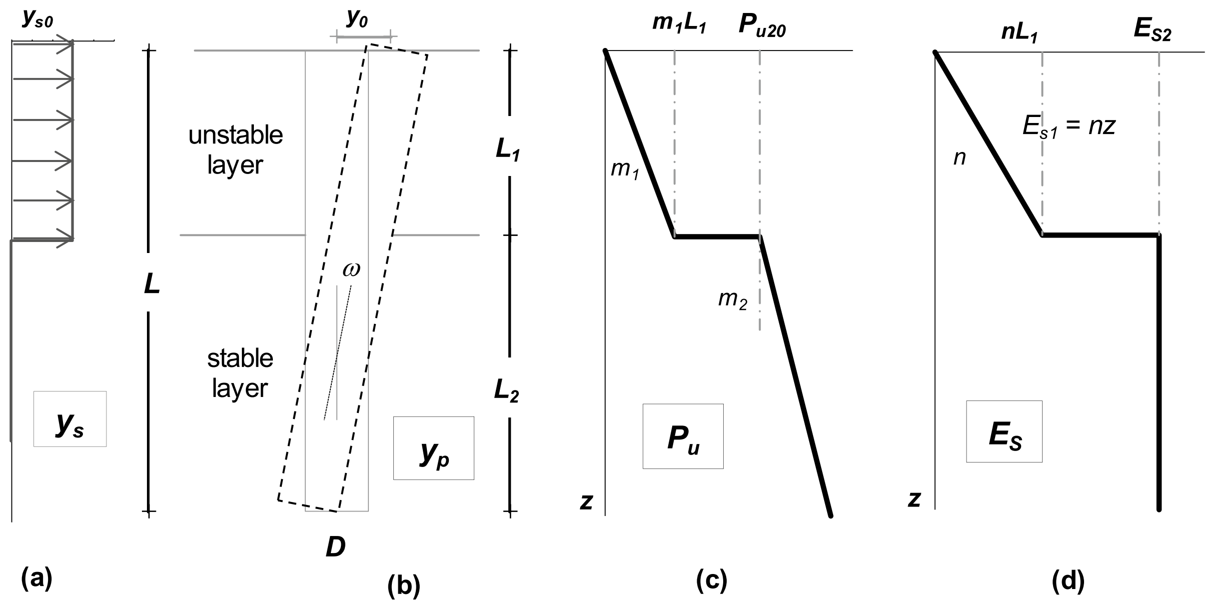

Fig. 1 Basic assumptions of the proposed method: **a** soil movement; **b** rigid pile deformation; **c** variation of P_u with depth and **d** variation of E_S with depth

$$P_{u2} = P_{u20} + m_2(z - L_1) \tag{6}$$

where P_{u20} is the ultimate soil resistance at the top of the stable layer and m_2 is the gradient of P_{u2}.

The assumption of a uniform E_s is generally acceptable for overconsolidated clays (Terzaghi 1955; Viggiani et al. 2012; Zhang & Ahmari 2013).

The appropriate selection of the horizontal modulus of subgrade and limiting lateral soil pressure, although fundamental for the analysis, will not be discussed in this paper. Some suggestions for the choice of P_u values for both isolated pile and pile group can be found in Ito and Matsui 1975; De Beer and Carpentier 1977; Poulos (1995), Georgiadis et al. (2013). A comprehensive discussion on the selection of E_s for isolated piles is given by Zhang (2009) and Zhang and Ahmari (2013).

The method does not consider the formation of plastic hinge along the pile shaft; the absence of plastic hinges can be achieved by a proper design of the pile section and reinforcement based on the maximum moment provided by the analysis.

Finally, the assumption of a rigid deformation of the pile holds for particular combinations of pile flexural stiffness, mechanical properties of both unstable and stable layers and relative embedment lengths (L_1 and L_2). However, for practical purpose, the following condition can be used for a rough, but conservative, check of pile rigidity:

$$L < 2 \cdot \sqrt[4]{\frac{E_P J_P}{E_{s2}}} \tag{7}$$

where E_p is the pile elastic modulus of pile and J_P is the moment of inertia of pile cross sectional area.

Numerical analyses performed by the author confirm that when the condition (7) is met the pile behaves as a rigid one.

2.1 Dimensionless Parameters

The results of the present study are expressed in terms of dimensionless parameters.

The pile length L is defined by the embedment ratio λ:

$$\lambda = L_2 / L_1 \tag{8a}$$

$$L_n = L / L_1 = 1 + \lambda \tag{8b}$$

The distributions of E_s and P_u with depth are described by R_E, R_U and ρ, defined as:

$$R_E = E_{S2} / nL_1 \tag{9a}$$

$$R_U = P_{u20} / m_1 L_1 \tag{9b}$$

$$\rho = m_2 / m_1 \tag{9c}$$

As shown in Fig. 1c-d, the parameters R_U and R_E are the ratio of E_s and P_u at the layer interface, respectively.

The shear force mobilized at the sliding depth (which essentially gives the main contribution of a row of passive piles in slope stability) is expressed by:

$$T_{sn} = \frac{T_s}{m_1 L_1^2} \tag{10}$$

In such a way $T_{sn} = 0.5$ when the horizontal soil resistance of the unstable layer is fully mobilized.

Similarly, the maximum bending moment along the pile shaft (useful for structural design of passive piles) is normalized as:

$$M_{\max n} = \frac{M_{\max}}{m_1 L_1^3} \tag{11}$$

Finally, the soil movement, pile head displacement and pile rotation (useful for serviceability limit state analysis) are conveniently expressed by:

$$y_{s0n} = y_{s0} \frac{R_E n}{m_1} = y_{s0} \frac{E_{s2}}{m_1 L_1} \tag{12}$$

$$y_{0n} = y_0 \frac{R_E n}{m_1} = y_0 \frac{E_{s2}}{m_1 L_1} \tag{13}$$

$$\omega_n = \tan \omega \frac{R_E n L_1}{m_1} = \tan \omega \frac{E_{s2}}{m_1} \tag{14}$$

3 Results and Discussion

A passive pile is gradually loaded for increase of the soil movement. Referring to Soil–pile interaction three different conditions can be generally distinguished: (1) initially, for relatively small soil displacement an elastic condition is achieved for the entire length; (2) then, for soil movement exceeding a first threshold value, y_{s0ne}, an elastic–plastic condition is achieved with the soil at the ultimate state only in limited zones whose extent increases at increasing soil movements; (3) finally, for soil movement exceeding a second threshold value, y_{s0np}, a plastic condition can be achieved corresponding to the full plasticization of soil above and/or below the sliding depth. For the assumed distributions of soil movement and soil properties (Fig. 1), the extent of the elastic and elastic–plastic zones (i.e. the values of y_{s0ne} and y_{s0np}) depends on λ, R_E, R_U and ρ.

In the following paragraphs the above-mentioned cases (elastic, elastic–plastic and plastic) are analyzed separately with the aim to obtain, whenever possible, closed-form expressions useful for design purposes.

3.1 Elastic Case

On the basis of (1)-(4), the normalized elastic soil reaction versus depth can be expressed as:

$$P_{en} = \frac{P_e}{m_1 L_1} = \begin{cases} \left(\omega_n z_n^2 - \Delta y_{0n} \cdot z_n\right) / R_E & 0 \le z_n \le 1 \\ \omega_n z_n - y_{0n} & 1 \le z_n \le L_n \end{cases} \tag{15}$$

where $\Delta y_{0n} = \left(y_{0n} - y_{s0n}\right)$ and $z_n = z/L_1$.

Imposing the horizontal force equilibrium and the moment equilibrium about the pile head, a linear system of two variables is obtained:

$$\frac{1}{2}\left(y_{0n} - y_{s0n}\right) - \frac{1}{3}\omega_n + y_{0n}\left(L_n - 1\right)R_E - \frac{1}{2}\omega_n\left(L_n^2 - 1\right)R_E = 0 \tag{16}$$

$$\frac{1}{3}\left(y_{0n} - y_{s0n}\right) - \frac{1}{4}\omega_n + \frac{1}{2}y_{0n}\left(L_n^2 - 1\right)R_E - \frac{1}{3}\omega_n\left(L_n^3 - 1\right)R_E = 0 \tag{17}$$

The analytical solution in dimensionless form is found to be:

$$y_{0n} = \frac{1 + 12R_E\lambda(1+\lambda)^2}{1 + 6R_E^2\lambda^4 + 6R_E\lambda\left(1 + 2\lambda + 2\lambda^2\right)} y_{s0n} \tag{18}$$

$$\omega_n = \frac{6R_E\lambda(2 + 3\lambda)}{1 + 6R_E^2\lambda^4 + 6R_E\lambda\left(1 + 2\lambda + 2\lambda^2\right)} y_{s0n} \tag{19}$$

Once y_{0n} and ω_n have been obtained, the internal forces at any depth can be calculated by the expressions listed in Table 1. An example of the distribution of the

Table 1 Internal forces for the elastic case

range	Normalised shear force T and bending moment M
$0 \leq z_n \leq 1$	$T_n = \frac{T}{m_1 L_1^2} = -\frac{\Delta y_{0n}}{2R_E} z_n^2 + \frac{\omega_n}{3R_E} z_n^3 \quad \Delta y_{0n} = \left(y_0 - y_s\right)\frac{nR_E}{m_1} \quad z_n = z/L_1$
	$M_n = \frac{M}{m_1 L_1^3} = -\frac{\Delta y_{0n}}{6R_E} z_n^3 + \frac{\omega_n}{12R_E} z_n^4$
	M_{max} at $\frac{z_{m1}}{L_1} = \frac{3}{2}\frac{\Delta y_{0n}}{\omega_n}$ provided that $0 < \frac{z_{m1}}{L_1} < 1$
$1 \leq z_n \leq L_n$	$T_n = -y_{0n}\left(z_n - L_n\right) + \frac{1}{2}\omega_n\left(z_n^2 - L_n^2\right)$
	$M_n = -\frac{1}{2}y_{0n}\left(z_n - L_n\right)^2 + \frac{1}{6}\omega_n\left(z_n^3 - 3L_n^2 z_n + 2L_n^3\right)$
	M_{max} at $\frac{z_{m2}}{L_1} = \frac{2y_{0n}}{\omega_n} - L_n$ provided that $1 < \frac{z_{m2}}{L_1} < L_n$

soil reaction, shear force and bending moment is shown in Fig. 2.

In the presence of a uniform soil movement the shear force (Fig. 2c) achieves a relative maximum at the depth of sliding ($z_n = 1$) and it can be calculated as:

$$T_{sn} = y_{0n}\lambda - \frac{1}{2}\omega_n\lambda(2 + \lambda) \tag{20}$$

After rearranging the terms, taking into account Eqs. (18)-(19), the following linear relationships can be derived:

$$T_{sn} = f_{Tys} \cdot y_{s0n} \tag{21}$$

$$y_{0n} = f_{yT} \cdot T_{sn} \tag{22}$$

where $f_{Tys} = \frac{\lambda + 3R_E\lambda^4}{1 + 6R_E^2\lambda^4 + 6R_E\lambda\left(1 + 2\lambda + 2\lambda^2\right)}$

and $f_{yT} = \frac{1 + 12R_E\lambda(1+\lambda)^2}{\lambda + 3R_E\lambda^4}$.

The bending moment can peak both above and below the sliding surface depending on the combinations of the values of λ and R_E. Then, the maximum bending moment is obtained as

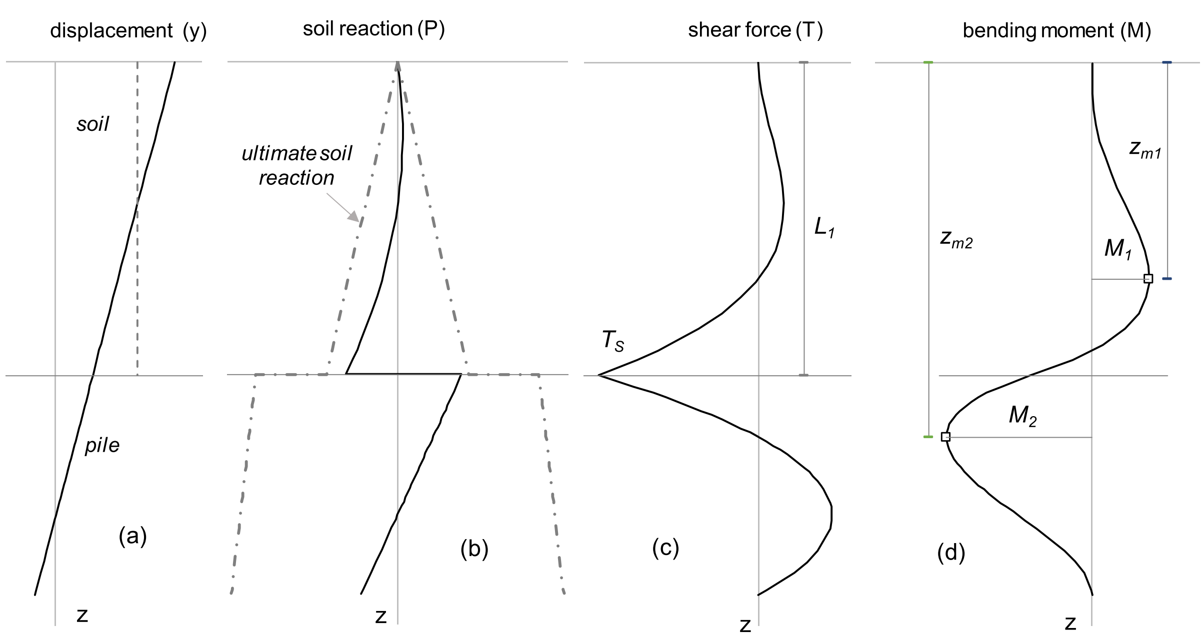

Fig. 2 Example of the elastic response of a rigid passive pile subjected to a uniform soil movement: **a** pile and soil displacement; **b** soil reaction; **c** shear force **d** bending moment

$$M_{\max,n} = \max\left\{\left|M_{1n}\right|;M_{2n}\right\} = \max\left\{\frac{9\Delta y_{0n}^4}{64R_E\omega_n^3};\frac{2\omega_n}{3}\left(L_n-\frac{y_{0n}}{\omega_n}\right)^3\right\} \quad (23)$$

where M_{1n} and M_{2n} are the maximum bending moment above and below the sliding surface, respectively (Fig. 2d).

For values of the embedment ratio of practical interest the maximum moment is always achieved in the stable zone (see Fig. 2d). Then, rearranging (23) taking into account of (18), (19) and (20), a linear correlation between M_{maxn} and T_{sn} can be obtained:

$$M_{\max n} = f_{MT}\cdot T_{sn} \quad (24)$$

where $f_{MT} = \frac{\left[1+\lambda-\left(6R_E\lambda^2\right)^{-1}\right]^3}{(1+1.5\lambda)^2\left[3+\left(R_E\lambda^3\right)^{-1}\right]}$

3.2 Elastic–Plastic Cases

By combining different values of y_s, λ, R_E, R_U and ρ various elastic–plastic (*EP*) cases can occur. The simplest cases are those in which soil reaction reaches its ultimate value only in one zone (Fig. 3a, b). For increasing soil movement more complex cases can develop, where two, three or four zones are simultaneously in plastic state (Fig. 3c, d, e).

A generalized *EP*-case is here comprehensively analyzed assuming a combination of the input parameters y_s, λ, R_E, R_U and ρ for which the soil reaches the ultimate value in four zones, as shown in Fig. 3e.

Horizontal and rotational equilibrium are assured when:

$$\begin{aligned}&-\frac{1}{2}b_n^2-\frac{1}{2R_E}\left(y_{0n}-y_{s0n}\right)\left(c_n^2-b_n^2\right)+\frac{1}{3R_E}\omega_n\left(c_n^3-b_n^3\right)\\&+\frac{1}{2}\left(1-c_n^2\right)-R_U\left(f_n-1\right)-\frac{1}{2}\rho\left(f_n-1\right)^2-y_{0n}\left(g_n-f_n\right)\\&+\frac{1}{2}\omega_n\left(g_n^2-f_n^2\right)+R_U\left(L_n-g_n\right)+\frac{1}{2}\rho\left(L_n-1\right)^2-\frac{1}{2}\rho\left(g_n-1\right)^2=0\end{aligned} \quad (25)$$

$$\begin{aligned}&-\frac{1}{3}b_n^3-\frac{1}{3R_E}\left(y_{0n}-y_{s0n}\right)\left(c_n^3-b_n^3\right)+\frac{1}{4R_E}\omega_n\left(c_n^4-b_n^4\right)\\&+\frac{1}{3}\left(1-c_n^3\right)-\frac{1}{2}R_U\left(f_n^2-1\right)-\frac{1}{3}\rho\left(f_n^3-1\right)+\frac{1}{2}\rho\left(f_n^2-1\right)\\&-\frac{1}{2}y_{0n}\left(g_n^2-f_n^2\right)+\frac{1}{3}\omega_n\left(g_n^3-f_n^3\right)+\frac{1}{2}R_U\left(L_n^2-g_n^2\right)\\&+\frac{1}{3}\rho\left(L_n^3-g_n^3\right)-\frac{1}{2}\rho\left(L_n^2-g_n^2\right)=0\end{aligned} \quad (26)$$

where b_n, c_n, f_n and g_n are the normalized depths that define the extent of the plastic zones (Fig. 3e).

By equalizing elastic soil reaction (P_e) and ultimate resistance per unit length (P_u) the following expressions can be derived:

$$b_n=\frac{b}{L_1}=\frac{y_{0n}-y_{s0n}-R_E}{\omega_n} \quad (27)$$

$$c_n=\frac{c}{L_1}=\frac{y_{0n}-y_{s0n}+R_E}{\omega_n} \quad (28)$$

$$f_n=\frac{f}{L_1}=\frac{y_{0n}-R_U+\rho}{\omega_n+\rho} \quad (29)$$

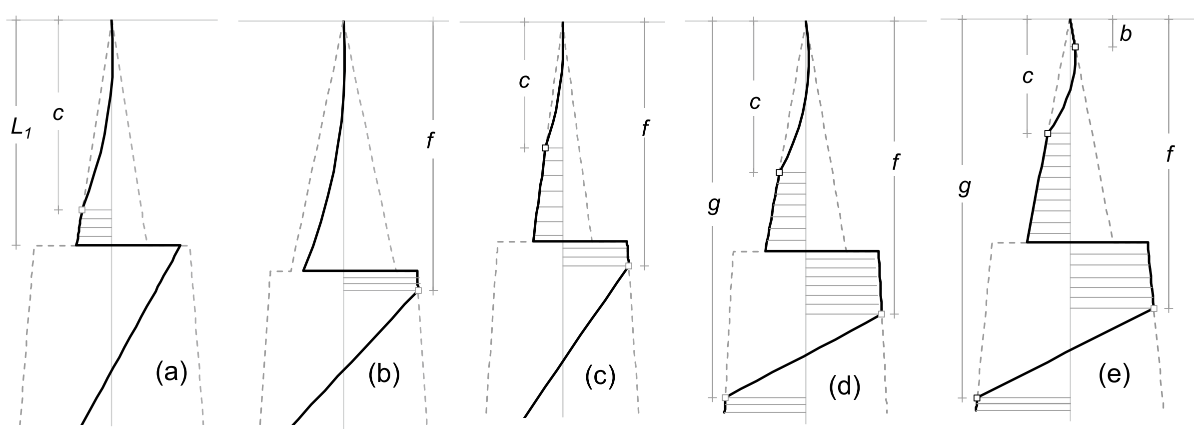

Fig. 3 Soil reaction in some elastic–plastic cases: **a** one plastic zone above the sliding surface; **b** one plastic zone below the sliding surface; **c** two plastic zones above and below the sliding surface; **d** three plastic zones above and below the sliding surface and on tip; **e** generalized case with four plastic zones

Table 2 Internal forces for the generalized elastic–plastic case

Range	Normalized shear force T and bending moment M
$0 \le z \le b_n$	$T_n = \frac{T}{mL_1^2} = -\frac{1}{2}z_n^2 \quad M_n = \frac{M}{mL_1^3} = -\frac{1}{6}z_n^3$
$b_n \le z_n \le c_n$	$T_n = -\frac{1}{2}b_n^2 - \frac{\Delta y_{0n}}{2R_E}\left(z_n^2 - b_n^2\right) + \frac{\omega_n}{3R_E}\left(z_n^3 - b_n^3\right) \; \Delta y_{0n} = y_{0n} - y_{s0n} \quad M_n = -\frac{1}{6}b_n^2\left(3z_n - 2b_n\right) - \frac{\Delta y_{0n}}{6R_E}\left(z_n^3 - 3b_n^2 z_n + 2b_n^3\right) + \frac{\omega_n}{12R_E}\left(z_n^4 - 4b_n^3 z_n + 3b_n^4\right)$
	The depth M_{max} at. z_{m1} is the solution of a 3-order equation: $z_{m1n}^3 - 1.5\frac{\Delta y_{0n}}{\omega_n}z_{m1n}^2 + \left\{1.5b_n^2\frac{\Delta y_{0n}}{\omega_n} - b_n^3 - \frac{1.5R_E b_n^2}{\omega_n}\right\} = 0$ provided that $b_n \le \frac{z_{m1}}{L_1} \le c_n$
$c_n \le z_n \le 1$	$T_n = \frac{1}{2}\left(z_n^2 - c_n^2 - b_n^2\right) - \frac{\Delta y_{0n}}{2R_E}\left(c_n^2 - b_n^2\right) + \frac{\omega_n}{3R_E}\left(c_n^3 - b_n^3\right)$
	$M_n = \frac{1}{6}\left\{z_n^3 - 3\left(b_n^2 + c_n^2\right)z_n + 2\left(c_n^3 + b_n^3\right)\right\} - \frac{\Delta y_{0n}}{6R_E}\left\{3\left(c_n^2 - b_n^2\right)z_n - 2\left(c_n^3 - b_n^3\right)\right\}$
	$+\frac{\omega_n}{12R_E}\left\{4\left(c_n^3 - b_n^3\right)z_n - 3\left(c_n^4 - b_n^4\right)\right\}$
	M_{max} at depth $\frac{z_{m1}}{L_1} = \sqrt{c_n^2 + b_n^2 + \frac{\Delta y_{0n}}{R_E}\left(c_n^2 - b_n^2\right) - \frac{2}{3}\frac{\omega_n}{R_E}\left(c_n^3 - b_n^3\right)}$ provided that $c_n \le \frac{z_{m1}}{L_1} \le 1$
$1 \le z_n \le f_n$	$T_n = -R_U\left(z_n - f_n - g_n + L_n\right) + y_{0n}\left(g_n - f_n\right) - \frac{1}{2}\omega_n\left(g_n^2 - f_n^2\right) - \frac{1}{2}\rho\left[\left(z_n - 1\right)^2 - \left(g_n - 1\right)^2 - \left(f_n - 1\right)^2 + \lambda^2\right]$
	$M_n = -\frac{1}{2}R_U\left[z_n^2 + f_n^2 + g_n^2 - L_n^2 - 2\left(f_n + g_n - L_n\right)z_n\right] - \frac{1}{2}y_{0n}\left[g_n^2 - f_n^2 - 2\left(g_n - f_n\right)z_n\right]$
	$+\omega_n\left[\frac{1}{3}\left(g_n^3 - f_n^3\right) - \frac{1}{2}\left(g_n^2 - f_n^2\right)z_n\right] - \frac{1}{2}\rho\left\{\begin{array}{l}\frac{1}{3}\left[\left(z_n - 1\right)^3 - \left(f_n - 1\right)^3 - \left(g_n - 1\right)^3 + \lambda^3\right] + \lambda^2\left(z_n - L_n\right)\\ -\left(g_n - 1\right)^2\left(z_n - g_n\right) - \left(f_n - 1\right)^2\left(z_n - f_n\right)\end{array}\right\}$
	$M_{max\text{ at }}\frac{z_{m2}}{L_1} = \frac{\rho - R_U + \sqrt{\left(R_U - \rho\right)^2 - \rho C_P}}{\rho} \le f_n \; C_P = \left\{\begin{array}{l}\left(g_n^2 - f_n^2\right)\omega_n - 2\left(g_n - f_n\right)y_{0n} + 2R_U\left(L_n - f_n - g_n\right)\\ -\rho\left[\left(g_n - 1\right)^2 + \left(f_n - 1\right)^2 - \lambda^2 - 1\right]\end{array}\right\}$
$f_n \le z_n \le g_n$	$T_n = R_U\left(g_n - L_n\right) - y_{0n}\left(z_n - g_n\right) + \frac{1}{2}\omega_n\left(z_n^2 - g_n^2\right) + \frac{1}{2}\rho\left[\left(g_n - 1\right)^2 - \lambda^2\right]$
	$M_n = \frac{1}{2}R_U\left(L_n - g_n\right)\left(L_n + g_n - 2z_n\right) - \frac{1}{2}y_{0n}\left(z_n - g_n\right)^2 + \frac{1}{6}\omega_n\left(z_n^3 - 3g_n^2 z_n + 2g_n^3\right)$
	$+\frac{1}{2}\rho\left\{\left(g_n - 1\right)^2\left(z_n - g_n\right) + \lambda^2\left(L_n - z_n\right) + \frac{1}{3}\left[\left(g_n - 1\right)^3 - \lambda^3\right]\right\}$
	M_{max} at $\frac{z_{m2}}{L_1} = \frac{y_{0n} - \sqrt{y_{0n}^2 - \omega_n C_E}}{\omega_n} \ge f_n \; C_E = 2R_U\left(g_n - L_n\right) + 2y_{0n}g_n - \omega_n g_n^2 + \rho\left[\left(g_n - 1\right)^2 - \lambda^2\right]$
$g_n \le z_n \le L_n$	$T_n = R_U\left(z_n - L_n\right) + 0.5\rho\left[\left(z_n - 1\right)^2 - \lambda^2\right]$
	$M_n = \frac{1}{2}R_U\left(z_n - L_n\right)^2 + \frac{1}{6}\rho\left[\left(z_n - 1\right)^3 - \lambda^3\right] - \frac{1}{2}\rho\lambda^2\left(z_n - L_n\right)$

$$g_n = \frac{g}{L_1} = \frac{y_{0n} + R_U - \rho}{\omega_n - \rho} \tag{30}$$

Equations (25–30) represent a nonlinear system of 6 equations in 6 variables (y_{0n}, ω_n, b_n, c_n, f_n and g_n). The solution of this system cannot be obtained in closed form, but it can be readily accomplished by simple spreadsheet software (e.g. the tool *Solver* of *Microsoft Excel*).

On the basis of y_{0n} and ω_n, the shear force and bending moment can be computed by the expressions listed in Table 2. The normalized shear force at the sliding depth can be obtained as:

$$T_{sn} = R_U(f_n + g_n - \lambda - 2) - \frac{1}{2}\rho\left[\lambda^2 - (g_n - 1)^2 - (f_n - 1)^2\right] + y_{0n}(g_n - f_n) - \frac{1}{2}\omega_n(g_n^2 - f_n^2) \tag{31}$$

It is worth to note that all possible elastic–plastic cases can be viewed as special cases of that described above. For example, the case with two yielded zones above and below L_1 (Fig. 3c) can be analyzed simplifying (25) and (26), as well as the expressions of Table 2, by putting $b_n = 0$ and $g_n = L_n$ and solving a nonlinear system with 4 variables (y_{0n}, ω_n, c_n, and f_n).

3.3 Elastic Thresholds

For the assumed distributions of P_u, E_s and y_s the zone of first plasticization is found to generally occur immediately above (Fig. 3a) or below (Fig. 3b); only for very low embedment ratios the first plasticization can occur at the pile head. The relevant limiting soil displacement (y_{s0nA}, y_{s0nB} and y_{s0nH}) can be obtained by imposing $c_n = 1$ in (28), $f_n = 1$ in (29) and $b_n = 0$

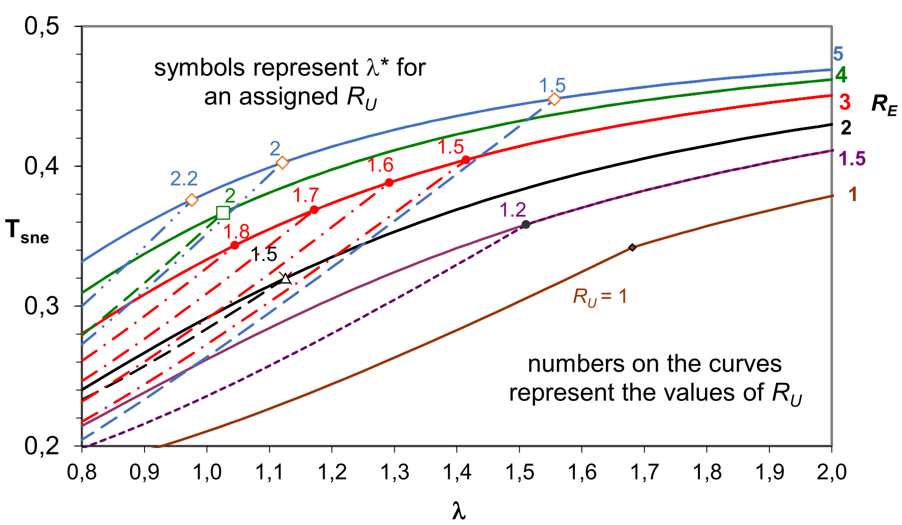

Fig. 4 Influence of λ, R_E and R_U on the shear force at the sliding surface at the elastic threshold

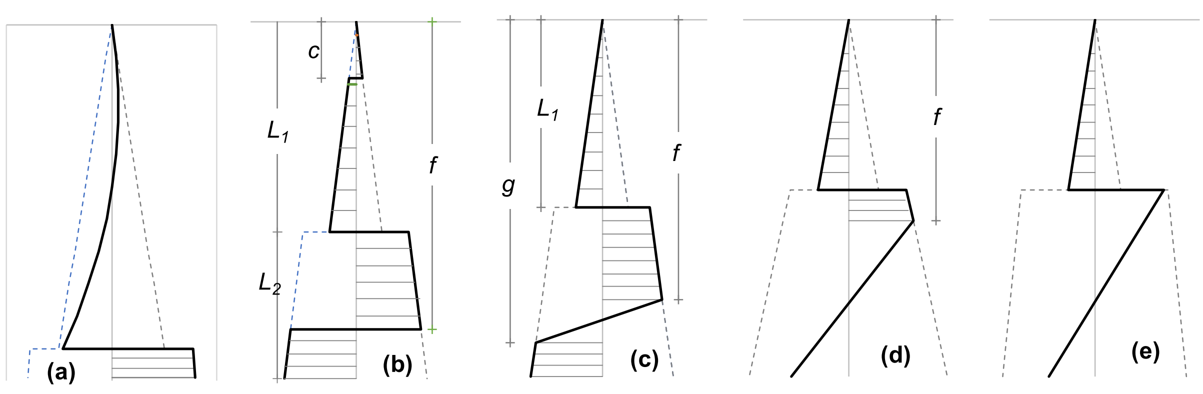

Fig. 5 Soil reaction distribution for plastic cases: **a** mode A; **b** mode B; **c** mode C1; **d** mode C2; **e** mode C3

in (27), respectively. Taking into account of (18) and (19), the following values are computed:

$$y_{s0n,A} = \frac{1 + 6R_E^2\lambda^4 + 6R_E\lambda\left(1 + 2\lambda + 2\lambda^2\right)}{6R_E\lambda^4 + 6\lambda(1 + \lambda)} \tag{32a}$$

$$y_{s0n,B} = \frac{1 + 6R_E^2\lambda^4 + 6R_E\lambda\left(1 + 2\lambda + 2\lambda^2\right)}{1 + 6R_E\lambda^2(1 + 2\lambda)}R_U \tag{32b}$$

$$y_{s0n,H} = \frac{1 + 6R_E^2\lambda^4 + 6R_E\lambda\left(1 + 2\lambda + 2\lambda^2\right)}{6\lambda(1 + 2\lambda) - 6R_E\lambda^4} \tag{32c}$$

The elastic threshold is taken as the minimum (positive) among the above values.

$$y_{s0ne} = \min\left\{y_{s0nA};y_{s0nB};y_{s0nH}\right\} \tag{33}$$

The pile head deflection, shear force at the sliding surface T_{sne} and the maximum bending moment M_{maxne} relevant to the elastic threshold can be obtained by substituting y_{s0ne} into (18), (20) and (24), respectively.

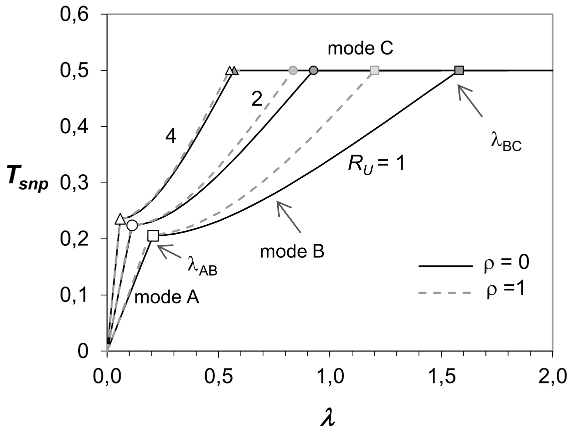

Fig. 6 Influence of λ, R_U and ρ on the normalized shear force at the sliding depth in plastic conditions

Table 3 Analytical equations for failure mode B

Conditions of existence

$\Delta \le 0$ where $\Delta = B^2 - AC$ $\quad A = 4R_U^2 + 2\rho X \quad B = R_U X - \rho Y \quad C = X^2 + 2R_U Y \quad X = 1 + 2R_U\lambda + \rho\lambda^2 \quad Y = 1 - 3R_U\lambda^2 - 2\rho\lambda^3$

Equilibrium equations

$$-\tfrac{1}{2}c_n^2 + \tfrac{1}{2}\left(1 - c_n^2\right) - R_U\left(f_n - 1\right) - \tfrac{1}{2}\rho\left(f_n - 1\right)^2 + R_U\left(L_n - f_n\right) + \tfrac{1}{2}\rho\left(L_n - 1\right)^2 - \tfrac{1}{2}\rho\left(f_n - 1\right)^2 = 0$$

$$-\frac{1}{3}c_n^3 + \frac{1}{3}\left(1 - c_n^3\right) - \frac{1}{2}R_U\left(f_n^2 - 1\right) - \frac{1}{3}\rho\left(f_n^3 - 1\right) + \frac{1}{2}\rho\left(f_n^2 - 1\right) + \frac{1}{2}R_U\left(L_n^2 - f_n^2\right) + \frac{1}{3}\rho\left(L_n^3 - f_n^3\right) - \frac{1}{2}\rho\left(L_n^2 - f_n^2\right) = 0$$

Internal forces

$$T_n = \begin{cases} -0.5z_n^2 & 0 \le z_n \le c_n \\ 0.5z_n^2 - c_n^2 & c_n \le z_n \le 1 \\ -R_U\left(z_n - 2f_n + L_n\right) - 0.5\rho\left[\left(z_n - 1\right)^2 - 2\left(f_n - 1\right)^2 + \lambda^2\right] & 1 \le z_n \le f_n \\ R_U\left(z_n - L_n\right) + 0.5\rho\left[\left(z_n - 1\right)^2 - \lambda^2\right] & f_n \le z_n \le L_n \end{cases}$$

$$M_n = \begin{cases} -z_n^3/6 & 0 \le z_n \le c_n \\ \left(z_n^3 - 6c_n^2 z_n + 4c_n^3\right)/6 & c_n \le z_n \le 1 \\ \left\{\begin{array}{l} -\frac{1}{2}R_U\left[z_n^2 + 2f_n^2 - L_n^2 - 2\left(2f_n - L_n\right)z_n\right] - \frac{1}{6}\rho\left[\left(z_n - 1\right)^3 - 2\left(f_n - 1\right)^3 + \lambda^3\right] \\ -\frac{1}{2}\rho\left[\lambda^2\left(z_n - L_n\right) + 2\left(f_n - 1\right)^2\left(z_n - f_n\right)\right] \end{array}\right\} & 1 \le z_n \le f_n \\ \frac{1}{2}R_U\left(z_n - L_n\right)^2 - \frac{1}{2}\rho\lambda^2\left(z_n - L_n\right) + \frac{1}{6}\rho\left[\left(z_n - 1\right)^3 - \lambda^3\right] & f_n \le z_n \le L_n \end{cases}$$

M_{max} at depth $\frac{z_{m2}}{L_1} = \frac{\rho - R_U + \sqrt{\left(R_U - \rho\right)^2 + \rho C_P}}{\rho} \qquad C_P = \begin{bmatrix} 2R_U\left(2f_n - L_n\right) - \rho \\ +2\rho\left(f_n - 1\right)^2 - \rho\lambda^2 \end{bmatrix}$

In Fig. 4 the values of the normalized shear force at the elastic threshold T_{sne} are plotted against the embedment ratio for various combinations of R_E and R_U. It is evident that T_{sne} monotonically increases with λ regardless of the value of R_E and R_U. For an assigned value of R_U a limiting value of λ ($=\lambda^*$) exists beyond which T_{sne} depends only on R_E because the elastic threshold is governed by (32a) that does not include R_U. The value of λ^* decreases for increasing R_U. For $\lambda > \lambda^*$ T_{sne} increases with R_E (solid lines in Fig. 6); as an example, for $R_E = 5$ and $\lambda = 1.6$, T_{sne} is high as 0.45, i.e. the pile response is fully elastic until it reaches 90% of its maximum response. On the other hand for $\lambda < \lambda^*$ the elastic threshold is governed by (32b) and different curves of T_{sne} versus λ can be drawn at varying R_U (dashed lines in Fig. 4).

3.4 *Plastic Cases*

It is well recognized that, for a free head pile, all elastic–plastic cases converge in one of three failure mechanisms indicates as: short-pile mode or mode A, intermediate mode or mode B and flow mode or mode C (e.g. Viggiani 1981; Poulos 1995; Kanagasabai

Table 4 Analytical equations and closed-form solutions for failure mode C1

Conditions of Existence

$0 \le \Delta \le (A\lambda - B)^2$ where $\Delta = B^2 - AC$ $\quad A = 4R_U^2 + 2\rho X \quad B = R_U X - \rho Y \quad C = X^2 + 2R_U Y \quad X = 1 + 2R_U\lambda + \rho\lambda^2$
$Y = 1 - 3R_U\lambda^2 - 2\rho\lambda^3$

Governing Equations

$$\frac{1}{2} - R_U(f_n - 1) - \frac{1}{2}\rho(f_n - 1)^2 - (g_n - f_n)y_{0n} + \frac{1}{2}(g_n^2 - f_n^2)\omega_n + R_U(L_n - g_n) + \frac{1}{2}\rho(L_n - 1)^2 - \frac{1}{2}\rho(g_n - 1)^2 = 0$$

$$\frac{1}{3} - \frac{1}{2}R_U(f_n^2 - 1) + \frac{1}{2}\rho(f_n^2 - 1) - \frac{1}{3}\rho(f_n^3 - 1) - \frac{1}{2}(g_n^2 - f_n^2)y_{0n} + \frac{1}{3}(g_n^3 - f_n^3)\omega_n$$
$$+\frac{1}{2}R_U(L_n^2 - g_n^2) - \frac{1}{2}\rho(L_n^2 - g_n^2) + \frac{1}{3}\rho(L_n^3 - g_n^3) = 0$$

$$f_n = \frac{f}{L_1} = \frac{y_{0n} - R_U + \rho}{\omega_n + \rho} \quad g_n = \frac{g}{L_1} = \frac{y_{0n} + R_U - \rho}{\omega_n - \rho}$$

Solutions

$$y_{0n} = \frac{R_U(A+B) + \rho(B+C)}{\sqrt{\Delta}} \quad \omega_n = \frac{R_U A + \rho B}{\sqrt{\Delta}} \quad f_n = 1 + \frac{B - \sqrt{\Delta}}{A} \quad g_n = 1 + \frac{B + \sqrt{\Delta}}{A} \quad y_{s0np} = y_{0n} + R_E$$

Internal forces

$$T_n = \begin{cases} 0.5z_n^2 & 0 \le z_n \le 1 \\ 0.5 - R_U(z_n - 1) - 0.5\rho(z_n - 1)^2 & 1 \le z_n \le f_n \\ -y_{0n}(z_n - g_n) + 0.5\omega_n(z_n^2 - g_n^2) + R_U(g_n - L_n) + 0.5\rho\left[(g_n - 1)^2 - \lambda^2\right] & f_n \le z_n \le g_n \\ R_U(z_n - L_n) + 0.5\rho\left[(z_n - 1)^2 - \lambda^2\right] & g_n \le z_n \le L_n \end{cases}$$

$$M_n = \begin{cases} z_n^3/6 & 0 \le z_n \le 1 \\ 0.5(z_n - 1) - 0.5R_U(z_n - 1)^2 - \rho(z_n - 1)^3/6 + 1/6 & 1 \le z_n \le f_n \\ \left\{\begin{aligned} &-\frac{y_{0n}}{2}(z_n - g_n)^2 + \frac{\omega_n}{6}(z_n^3 - 3g_n^2 z_n + 2g_n^3) + \frac{R_U}{2}(g_n - L_n)(2z_n - g_n - L_n) \\ &+\frac{\rho}{6}\left[(g_n - 1)^3 - \lambda^3\right] + \frac{\rho}{2}\left[(g_n - 1)^2(z_n - g_n) - \lambda^2(z_n - L_n)\right] \end{aligned}\right\} & f_n \le z_n \le g_n \\ 0.5R_U(z_n - L_n)^2 + \frac{\rho}{6}\left[(z_n - 1)^3 - \lambda^3\right] - \frac{\rho}{2}\lambda^2(z_n - L_n) & g_n \le z_n \le L_n \end{cases}$$

$$M_{\max n} = \frac{1}{6} + \frac{2(R_U^2 + \rho)^{1.5} - 3\rho R_U - 2R_U^3}{6\rho^2} \quad \text{at depth} \quad \frac{z_{m2}}{L_1} = 1 + \frac{\sqrt{R_U^2 + \rho} - R_U}{\rho} \le f_n$$

Table 5 Analytical equations and closed-form solutions for failure mode C2

Conditions of existence

$R_U\lambda^2 - 2\lambda - 1 \le 0$ and $A\lambda^2 - 2B\lambda + C \le 0$ where $A = 4R_U^2 + 2\rho X \quad B = R_U X - \rho Y \quad C = X^2 + 2R_U Y \; X = 1 + 2R_U\lambda + \rho\lambda^2$
$Y = 1 - 3R_U\lambda^2 - 2\rho\lambda^3$

Equations

$$\tfrac{1}{2} - R_U(f_n - 1) - \tfrac{1}{2}\rho(f_n - 1)^2 - (L_n - f_n)y_{0n} + \tfrac{1}{2}(L_n^2 - f_n^2)\omega_n = 0$$
$$\tfrac{1}{3} - \tfrac{1}{2}(R_U - \rho)(f_n^2 - 1) - \tfrac{1}{3}\rho(f_n^3 - 1) - \tfrac{1}{2}(L_n^2 - f_n^2)y_{0n} + \tfrac{1}{3}(L_n^3 - f_n^3)\omega_n = 0$$
$$f_n = \frac{f}{L_1} = \frac{y_{0n} - R_U + \rho}{\omega_n + \rho}$$

Solutions

$$y_{0n} = \frac{\left[2(R_U + 1)\lambda - (R_U - \rho)\lambda^2\right]\left(\rho\lambda^2 + 2R_U\lambda - 1\right)^2}{\left(\rho\lambda^3 + 3R_U\lambda^2 - 3\lambda - 1\right)^2} + R_U - \rho \quad y_{s0np} = y_{0n} + R_E \quad \omega_n = \frac{\left(\rho\lambda^2 + 2R_U\lambda - 1\right)^3}{\left(\rho\lambda^3 + 3R_U\lambda^2 - 3\lambda - 1\right)^2} - \rho$$
$$f_n = \frac{2(R_U + 1)\lambda - (R_U - \rho)\lambda^2}{\rho\lambda^2 + 2R_U\lambda - 1}$$

Internal forces

$$T_n = \begin{cases} 0.5z_n^2 & 0 \le z_n \le 1 \\ 0.5 - R_U(z_n - 1) - 0.5\rho(z_n - 1)^2 & 1 \le z_n \le f_n \\ -y_{0n}(z_n - L_n) + 0.5\omega_n(z_n^2 - L_n^2) & f_n \le z_n \le L_n \end{cases}$$
$$M_n = \begin{cases} z_n^3/6 & 0 \le z_n \le 1 \\ 0.5(z_n - 1) - 0.5R_U(z_n - 1)^2 - \tfrac{1}{6}\rho(z_n - 1)^3 + 1/6 & 1 \le z_n \le f_n \\ -0.5y_{0n}(z_n - L_n)^2 + \omega_n(z_n^3 - 3L_n^2 z_n + 2L_n^3)/6 & f_n \le z_n \le L_n \end{cases}$$
$$M_{\max n} = \frac{1}{6} + \frac{2(R_U^2 + \rho)^{1.5} - 3\rho R_U - 2R_U^3}{6\rho^2} \text{ at depth } z_{mn} = \frac{z_{m2}}{L_1} = 1 + \frac{\sqrt{R_U^2 + \rho} - R_U}{\rho} \le f_n$$
$$\text{Otherwise } M_{\max n} = \tfrac{1}{6}(z_{mn} - L_n)^2\left[\omega_n(z_{mn} + 2L_n) - 3y_{0n}\right] \text{ at depth } z_{mn} = \left(\tfrac{2y_{0n}}{\omega_n} - L_n\right) \ge f_n$$

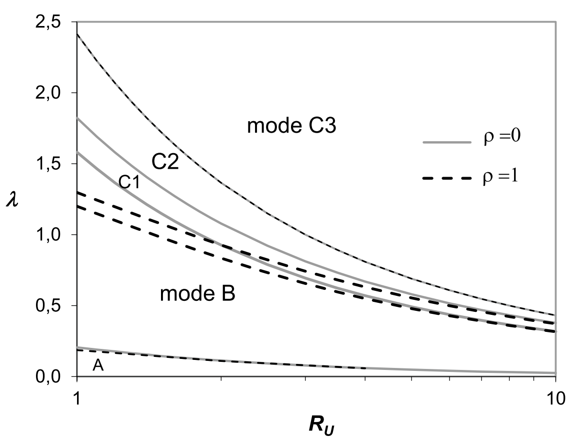

Fig. 7 Ranges of existence of different soil failure modes

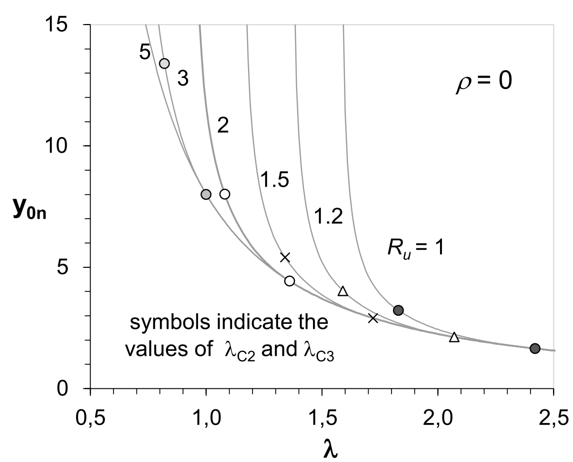

Fig. 8 Effect of λ and R_U on the normalized pile head deflection for failure mode C

Table 6 Analytical equations and closed-form solutions for failure mode C3

Condition of existence
$\lambda^2 R_U - 2\lambda - 1 > 0$
Equilibrium equations
$\frac{1}{2} - (L_n - 1)y_{0n} + \frac{1}{2}(L_n^2 - 1)\omega_n = 0$ $\frac{1}{3} - \frac{1}{2}(L_n^2 - 1)y_{0n} + \frac{1}{3}(L_n^3 - 1)\omega_n = 0$
Solutions
$y_{0n} = \frac{2(1+\lambda)^2}{\lambda^3}$ $\omega_n = \frac{2+3\lambda}{\lambda^3}$ $y_{s0n} = y_{0n} + R_E$
Internal forces
$T_n = \begin{cases} 0.5z_n^2 & 0 \le z_n \le 1 \\ -y_{0n}(z_n - L_n) + 0.5\omega_n(z_n^2 - L_n^2) & f_n \le z_n \le L_n \end{cases}$
$M_n = \begin{cases} z_n^3/6 & 0 \le z_n \le 1 \\ -0.5y_{0n}(z_n - L_n)^2 + \omega_n(z_n^3 - 3L_n^2 z_n + 2L_n^3)/6 & f_n \le z_n \le L_n \end{cases}$
$M_{\max n} = \frac{2(1+\lambda)^3}{3(2+3\lambda)^2}$ at depth $\frac{z_{m2}}{L_1} = 1 + \frac{\lambda^2}{2+3\lambda}$

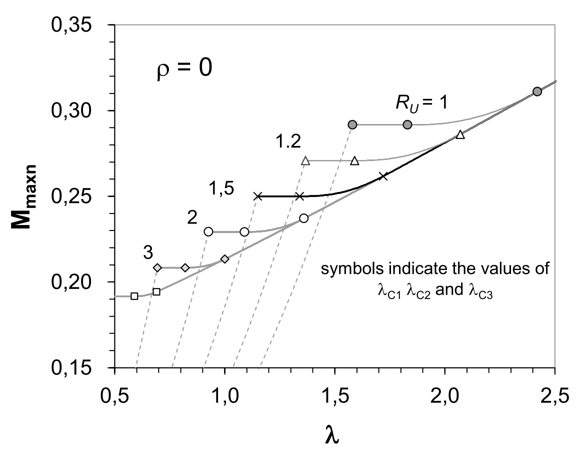

Fig. 9 Effect of λ and R_U on the normalized maximum bending moment

et al. 2011; Di Laora et al. 2017; Bellezza and Caferri 2018).

In mode A the slide is relatively deep (Fig. 5a) and there is full mobilization of strength in the stable soil (i.e. $f_n = g_n = L_n$ in eqs. 22 and 23), so that $T_{snp} = R_U \lambda + 0.5 \rho\lambda^2$. Mode A is of little practical interest in design and therefore it is marginally investigated in this paper.

In mode B the soil strength is fully mobilized both in the stable and unstable soil (Fig. 5b). This case can be analytically treated as a special case of the generalized EP case putting $b_n = c_n$ and $g_n = f_n$ in Eq. (25) and (26). The computation of the maximum shear force (T_{snp} = 0.5—c_n^2) is not straightforward, as the values of c_n and f_n must be numerically obtained by imposing horizontal and rotational equilibrium. The numerical solution has a practical meaning only when $0<b_n<1$ and $1<f_n<L_n$ and these conditions are met only for particular combinations of λ, R_U and ρ as detailed in Table 3.

Finally, in mode C the slide depth is relatively shallow and there is a full strength mobilization of the soil in the unstable layer, so that $T_{snp} = 0.5$ (Fig. 5c, d, e). The equilibrium equations are obtained by putting $b_n = c_n = 0$ in (22) and (23).

For an assigned combination of λ, R_U and ρ the normalized shear force at the sliding surface, $T_{sn,}$ is the minimum value among those relevant to mode A, mode B and mode C.

$$T_{snp} = \frac{T_s}{m_1 L_1^2} = \min\left\{R_U\lambda + 0.5\rho\lambda^2; 0.5 - c_n^2; 0.5\right\} \tag{34}$$

Figure 6 shows the trend of the normalized shear T_{snp} as a function of the embedment ratio λ for different values of R_U and ρ. For low values of λ mode A develops and T_{snp} increases linearly with λ; then, for λ greater than a first threshold value (λ_{AB}), mode B starts to govern the problem and the increase of T_{snp} is no more linear; finally, a second threshold value of λ (λ_{BC}) exists beyond which T_{snp} becomes independent of λ and R_U (mode C). The values of λ_{AB} and λ_{BC} are found to decrease with increasing R_U and ρ. The effect of ρ is appreciable only to low values of R_U.

Bellezza (2020) showed that within mode C three distinct sub-cases can be identified (C1, C2 and C3) which differ for the distribution of soil reaction in

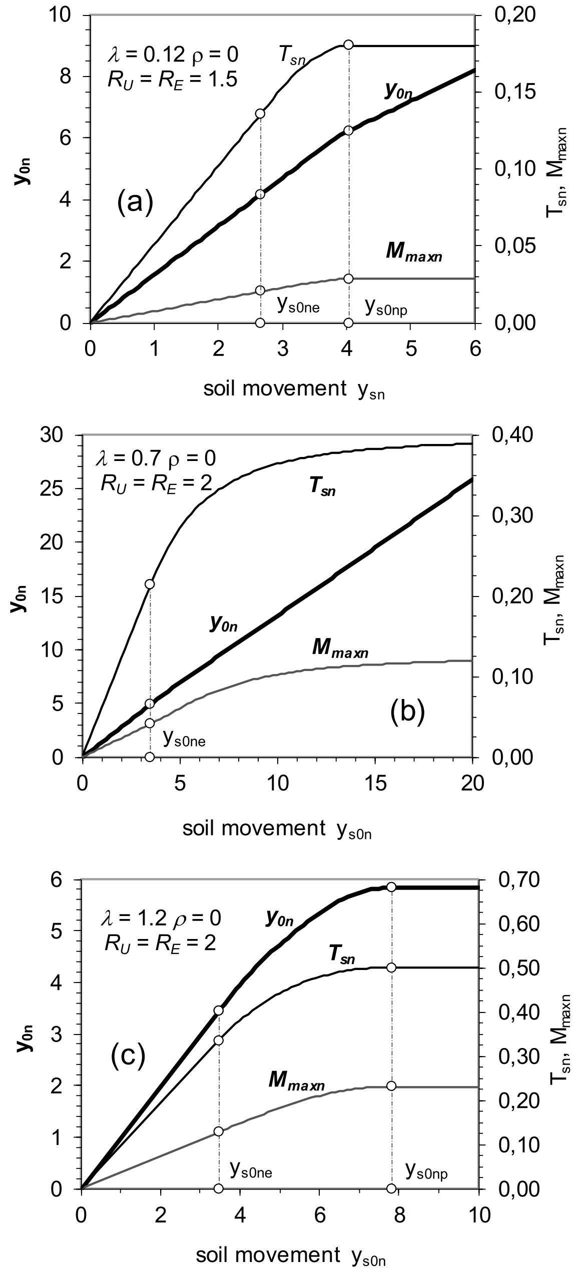

Fig. 10 Effect of the soil movement on the normalized shear force at the sliding depth (T_{sn}), maximum bending moment (M_{maxn}) and pile head deflection (y_{0n}) for three different combinations of λ, R_E,R_U and ρ: **a** $\lambda = 0.12$, $R_U = R_E = 1.5$, $\rho = 0$; **b** $\lambda = 0.7$ $R_U = R_E = 2$, $\rho = 0$; **c** $\lambda = 1.2$ $R_U = R_E = 2$ $\rho = 0$

the stable layer. In mode C1 the soil is in the plastic state both below the sliding surface and near the tip (Fig. 6c); in mode C2 there is only a plastic zone

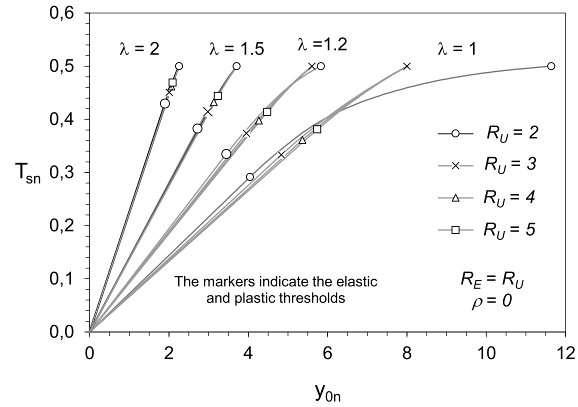

Fig. 11 Relationship between normalized shear force and pile head deflection for different combinations of λ, R_U R_E and ρ

below the sliding surface (Fig. 6d), whereas in mode C3 the soil remains elastic in the stable zone (Fig. 6e).

For each case (C1, C2 or C3) the governing equations can be algebraically manipulated to obtain closed-form expressions for normalized pile head displacement (y_{0n}), rotation (ω_n), limiting soil movement (y_{s0np}) and maximum bending moment (M_{maxn}), as well as the extent of the eventual plastic zone below the sliding surface (f_n and g_n). Tables 4–6 contain the governing expressions for mode C1, C2 and C3, respectively.

3.5 Thresholds Values of the Embedment Ratio

For the investigated soil profile, the transition value between mode A and mode B cannot be derived in closed form, but the value of λ_{AB} for $\rho = 0$ can be obtained by interpolating the numerical results as:

$$\lambda_{AB} \cong 0.211 \cdot R_U^{-0.918} \tag{35}$$

For $\rho > 0$ the values of λ_{AB} slightly decrease.

Also the ranges of occurrence of case C1 and C2 for $\rho > 0$ can be obtained only numerically on the basis of the expressions listed at the top of Tables 4–5. Only for $\rho = 0$ it is possible to obtain a set of closed-form expressions of the threshold values of λ for a given value of R_U (Bellezza 2020):

$$\lambda_{C1} = \lambda_{BC} = \frac{3 + \sqrt{18 + 24R_U}}{6R_U} \tag{36a}$$

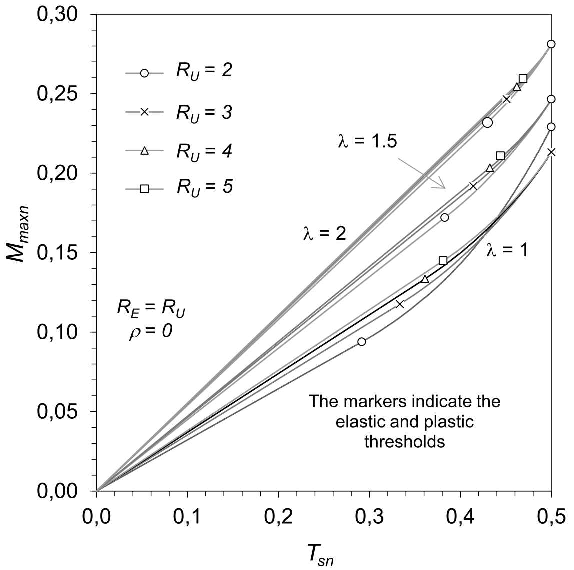

Fig. 12 Relationship between normalized shear force and maximum bending moment for different combinations of λ, R_U, R_E and ρ

$$\lambda_{C2} = \frac{1 + \sqrt{3 + 4R_U}}{2R_U} \tag{36b}$$

$$\lambda_{C3} = \frac{1 + \sqrt{1 + R_U}}{R_U} \tag{36c}$$

The last threshold value (λ_{C3}) is found to be independent of ρ, so that (36c) is valid also for $\rho > 0$.

Figure 7 shows the threshold values of λ plotted against R_U for two different values of ρ. It can be observed that λ_{C1} significantly decreases with R_U and consequently the range of existence of mode C greatly increases. As an example, for $R_U = 2.5$ and $\rho = 0$, $\lambda_{AB} = 0.091$, $\lambda_{C1} = \lambda_{BC} \approx 0.789$, $\lambda_{C2} \approx 0.921$ and $\lambda_{C3} \approx 1.148$. As expected, at increasing ρ, λ_{AB}, λ_{C1} and λ_{C2} decrease: for $R_U = 2.5$ and $\rho = 1$ $\lambda_{AB} \approx 0.090$, $\lambda_{C1} \approx 0.732$ and $\lambda_{C2} \approx 0.822$, whereas λ_{C3} remains unchanged, as the first plasticization occurs immediately below the sliding surface.

In Fig. 8 the values of the normalized pile head displacement y_{0n} are plotted as a function of the embedment ratio λ for different values of the strength ratio R_U and $\rho = 0$. For combinations of λ and R_U which implies the development of mode B, y_{0n} does not have a finite value and therefore all curves have a vertical asymptote in correspondence of λ_{C1}. Then, for $\lambda > \lambda_{BC}$, y_{0n} starts to decrease with λ. The rate of decrease of y_{0n} versus λ is initially very high and decreases at increasing λ according to the expression of Table 4; in the range of occurrence of mode C1 and C2, y_{0n} depends on λ, R_U and ρ (Tables 4–5). Finally, for $\lambda > \lambda_{C3}$ the normalized pile head displacement becomes independent of the plastic parameters R_U and ρ (see Table 6).

For a uniform distribution of y_s, the limiting soil movement required to reach the plastic case C can be obtained considering $c_n = 0$ in (25), i.e.

$$y_{s0np} = y_{0n} + R_E \tag{37}$$

Obviously, the value of y_{0n} in (37) is that pertaining to the case of occurrence (C1, C2 or C3).

Figure 9 shows the values of the normalized maximum bending moment M_{maxn} as a function of the embedment ratio λ for different value of R_U. In the investigated range of λ, for a given value of R_U, M_{maxn} first significantly increases with λ for mode B (dashed curves in Fig. 9); then, there is a small range of in which M_{maxn} is constant (mode C1) and finally M_{maxn} starts again to increase with λ at the occurrence of mode C2 and C3. For mode C3 the law of variation of M_{maxn} versus λ is the same, regardless of the value of R_U (see Table 6 for details).

4 Mobilization Curves

On the basis of the analysis developed in the previous sections, the shear force at the sliding depth T_{sn}, the maximum bending moment, M_{maxn}, and the pile head displacement, y_{0n}, can be calculated for any value of the soil movement, obtaining the so-called mobilization curves generally subdivided in elastic, elastic–plastic and plastic part. Figure 10 shows typical examples of mobilization curves relevant to three different combinations of λ, R_U and ρ which implies the final development of mode A, mode B and mode C, respectively. Note that for mode A (Fig. 10a) the plastic threshold of soil movement, y_{s0np}, exists; it is possible to demonstrate that for $y_{s0n} > y_{s0np}$, T_{sn} and M_{maxn} remain constant, but y_{0n} continues to increase with y_{s0n}, maintaining the same difference between y_{0n} and y_{s0n}. For mode B the plastic threshold does not exist; T_{sn} and M_{maxn} tend asymptotically to the plastic values of Table 3, whereas y_{0n} continue to increase

Table 7 Values of the normalized pile head displacement $y_{0n} \times 10^2$ for intermediate values of T_{sn}

λ	$R_E = R_U = 2$				$R_E = R_U = 3$				$R_E = R_U = 4$				$R_E = R_U = 5$			
	T_{sn}				T_{sn}				T_{sn}				T_{sn}			
	0.30	0.35	0.40	0.45	0.30	0.35	0.40	0.45	0.30	0.35	0.40	0.45	0.30	0.35	0.40	0.45
	$\rho = 0$															
0.7	758	1116	-(1)	-	791	968	1207	1666	825	991	1189	1419	854	1011	1200	1422
0.8	599	768	1139	-	632	757	903	1099	**658**(2)	775	914	1075	**676**	790	922	1078
0.9	493	596	764	1146	**520**	612	720	845	**537**	627	729	848	**547**	**638**	735	851
1.0	416	493	589	754	**435**	508	591	687	**445**	**520**	598	689	**452**	**527**	604	692
1.1	**356**	418	489	583	**369**	**431**	496	572	**376**	**438**	502	574	**380**	**443**	507	576
1.2	**309**	361	418	484	**317**	**370**	424	486	**322**	**375**	429	488	**325**	**379**	**433**	490
1.3	**270**	**315**	363	418	**276**	**322**	368	420	**279**	**326**	**373**	421	**281**	**328**	**375**	423
1.4	**239**	**278**	319	366	**243**	**283**	**324**	367	**245**	**286**	**328**	369	**246**	**288**	**329**	370
1.5	**213**	**248**	284	324	**216**	**252**	**288**	325	**217**	**254**	**290**	326	**218**	**255**	**291**	328
1.6	**191**	**223**	255	289	**193**	**226**	**258**	291	**194**	**227**	**260**	292	**195**	**228**	**260**	**293**
1.7	**173**	**202**	**230**	261	**175**	**204**	**233**	262	**175**	**205**	**234**	263	**176**	**205**	**235**	**264**
1.8	**157**	**184**	**210**	237	**159**	**185**	**211**	238	**159**	**186**	**213**	**239**	**160**	**186**	**213**	**240**
1.9	**144**	**168**	**192**	217	**145**	**169**	**193**	218	**146**	**170**	**195**	**219**	**146**	**170**	**194**	**219**
2.0	**133**	**155**	**177**	199	**133**	**156**	**178**	**200**	**134**	**156**	**179**	**201**	**134**	**156**	**179**	**201**
	$\rho = 1$															
0.7	756	1071	1893	-	791	968	1202	1616	825	991	1189	1419	854	1011	1200	1422
0.8	599	760	1057	1763	632	757	903	1095	**658**	775	914	1075	**676**	790	922	1078
0.9	493	595	749	1021	**520**	612	720	845	**537**	627	729	848	**547**	**638**	735	851
1.0	416	493	588	732	**435**	508	591	687	**445**	**520**	598	689	**452**	**527**	604	692
1.1	**356**	418	489	579	**369**	**431**	496	572	**376**	**438**	502	574	**380**	**443**	507	576
1.2	**309**	361	418	484	**317**	**370**	424	486	**322**	**375**	429	488	**325**	**379**	**433**	490

(1) the specified value of T_{sn} cannot be reached as mode B develops; (2) values in bold refer to the elastic soil response where closed-form expressions are available

monotonically with y_{s0n} (Fig. 10b). The final part of the curves can be obtained by numerically solving the generalized EP case (Fig. 5e). For mode C the pile head displacement and maximum bending moment remain constant after the plastic threshold and the pile response in terms of shear force at the sliding surface reaches its maximum (Fig. 10c). In such a case closed-form expressions are available also to evaluate both y_{0n} and M_{maxn} at the plastic threshold (Tables 4–6).

In design procedure the passive piles are requested to provide a stabilizing force needed to increase the factor of safety to the target value (Viggiani 1981; Poulos 1995). When the requested force for a single pile is less than the maximum one (i.e. $T_{snR} < 0.5$), pile response can fall in the elastic or in the elastic–plastic range and pile head deflection and the maximum bending moment are obviously less than those calculated in plastic conditions by the expressions obtained for mode C. For a fully elastic pile response (i.e. $T_{snR} < T_{sne}$) the closed-form expressions derived in this paper can be used for ready and accurate evaluations of the y_{0n} and M_{maxn} values. Conversely, in the elastic–plastic range (i.e. $T_{sne} < T_{snR} < 0.5$), closed-form expressions are not available and y_{0n} and M_{maxn} can be determined on the basis of the mobilization curves similar to those of Fig. 10. Considering that in design process more attention is focused on pile displacement and internal forces instead of soil movement, the mobilization curves of Fig. 11 can be conveniently drawn only in terms of y_{0n}, T_{sn} and M_{maxn}.

Figure 11 shows the values of T_{sn} as a function of y_{0n} for different combinations of λ and R_U with $R_E = R_U$ and $\rho = 0$.

It is evident that the mobilization curve is mainly influenced by the embedment ratio λ and slightly by R_U.

Table 8 Values of the normalized maximum bending moment × 10^3 for intermediate values of T_{sn}

λ	$R_E = R_U = 2$				$R_E = R_U = 3$				$R_E = R_U = 4$				$R_E = R_U = 5$			
	T_{sn}				T_{sn}				T_{sn}				T_{sn}			
	0.30	0.35	0.40	0.45	0.30	0.35	0.40	0.45	0.30	0.35	0.40	0.45	0.30	0.35	0.40	0.45
	$\rho = 0$															
0.7	67	94	- (1)	-	75	96	124	161	81	100	125	156	87	104	127	157
0.8	77	101	134	-	86	105	131	163	**93**(2)	110	133	163	**98**	114	136	164
0.9	87	108.0	138	178	**97**	114.6	139	169	**103**	120	142	170	**107**	**124**	144	171
1.0	97	117	143	180	**106**	124	146	175	**111**	**129**	150	177	**114**	**133**	153	178
1.1	**106**	125	150	183	**114**	**133**	154	182	**118**	**138**	158	184	**121**	**141**	161	185
1.2	**114**	134	157	188	**121**	**141**	162	189	**125**	**145**	166	191	**127**	**148**	**169**	192
1.3	**122**	**142**	165	195	**127**	**149**	170	196	**130**	**152**	**174**	198	**132**	**154**	**176**	199
1.4	**129**	**150**	173	201	**133**	**156**	**178**	204	**136**	**159**	**181**	205	**137**	**160**	**183**	207
1.5	**135**	**157**	180	208	**139**	**162**	**185**	211	**141**	**165**	**188**	213	**142**	**166**	**190**	214
1.6	**141**	**164**	198	215	**144**	**168**	**192**	218	**146**	**171**	**195**	220	**147**	**172**	**196**	**221**
1.7	**146**	**171**	**195**	222	**149**	**174**	**199**	225	**151**	**176**	**202**	227	**152**	**177**	**203**	**228**
1.8	**152**	**177**	**202**	230	**154**	**180**	**206**	232	**156**	**182**	**208**	**234**	**157**	**183**	**209**	**235**
1.9	**157**	**183**	**209**	237	**159**	**186**	**212**	239	**161**	**187**	**215**	**241**	**161**	**188**	**215**	**242**
2.0	**162**	**0.189**	**216**	244	**164**	**191**	**219**	**246**	**165**	**193**	**220**	**248**	**166**	**194**	**221**	**249**
	$\rho = 1$															
0.7	67	93	129	-	75	96	123	161	81	100	125	156	87	104	127	157
0.8	77	100	133	175	86	105	131	163	**93**	110	135	163	**98**	114	136	164
0.9	87	108	137	177	**97**	115	139	169	**103**	120	142	170	**107**	**124**	144	171
1.0	97	117	143	179	**106**	124	146	175	**111**	**129**	150	177	**114**	**133**	153	178
1.1	**106**	125	150	182	**114**	**133**	154	182	**118**	**138**	158	184	**121**	**141**	161	185
1.2	**114**	134	157	188	**121**	**141**	162	189	**125**	**145**	166	191	**127**	**148**	**169**	192

(1) the specified value of T_{sn} cannot be reached as mode B develops; (2) values in bold refer to the elastic soil response where closed-form expressions are available

The effect of R_U is appreciable only for low embedment ratios and when T_{sn} approaches its maximum value. For $\lambda = 1$ the curve for $R_U = 2$ is distinct from other ones; the difference is due to the different failure mode, i.e. for $R_U = 2$ mode C1 occurs, whereas for $R_U > 2.5$ mode C3 develops, at which a smaller pile head displacement occurs (see Table 4 and Table 6 for details). A similar trend is observed for $\lambda = 1.2$, but in this case the difference in the final values of y_{0n} is smaller because for $R_U = 2$ mode C2 develops (see Fig. 8). For higher embedment ratios ($\lambda = 1.5$ or $\lambda = 2$) mode C3 is always activated and all curves converge to the same final value of y_{0n} for all the investigated values of R_U. For higher embedment ratios the mobilization curves are practically superimposed, although the elastic thresholds are slightly different. On the other hand, for increasing embedment ratios it is always more difficult to satisfy the condition of pile rigidity.

Figure 12 shows the values of M_{maxn} as a function of T_{sn} for different combinations of λ and R_U with $R_E = R_U$ and $\rho = 0$.

The trend of the curves is similar: in the elastic range M_{maxn} linearly increases with T_{sn} (Eq. 24), whereas beyond the elastic threshold M_{maxn} increases nonlinearly, at increasing rates, with increasing T_{sn}. The slope of the curves in the elastic range, given by (24), significantly increases with the embedment ratio, whereas the effect of R_E is appreciable only for low values of λ. In the elastic–plastic range a crossover is evident for $\lambda = 1$ because the maximum bending moment for $R_E = R_U = 2$ is higher than that for $R_U \geq 3$ owing the different plastic mechanism (C1 and C3, respectively). On the contrary, for $\lambda = 1.5$ and $\lambda = 2$ all curves converge to the same final value of M_{maxn} relevant to case C3.

To obtain more accurate numerical values, Table 7 and Table 8 list the values of the normalized pile

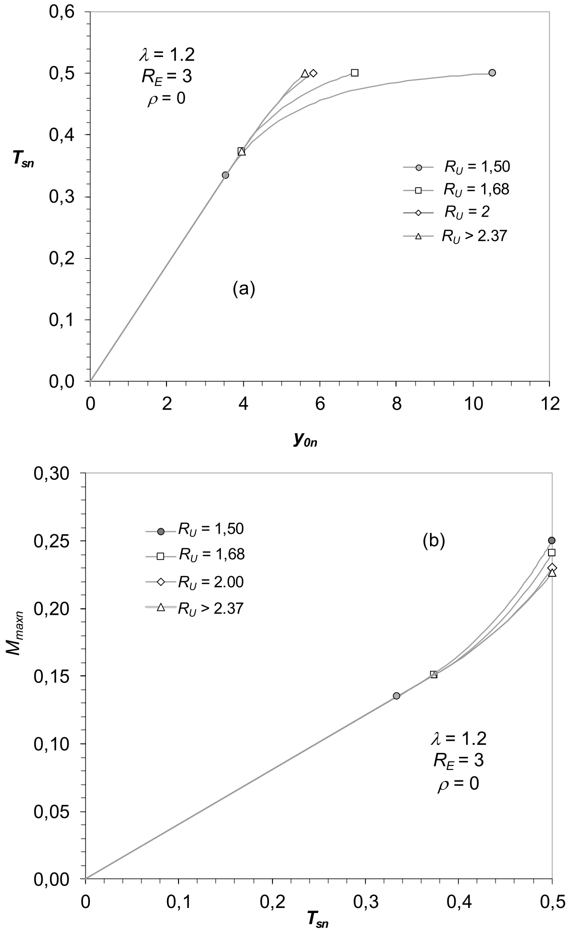

Fig. 13 Effect of R_U on the mobilization curve for $\lambda = 1.2$, $R_E = 3$ and $\rho = 0$: **a** T_{sn} *vs* y_{0n} **b** M_{maxn} *vs* T_{sn}

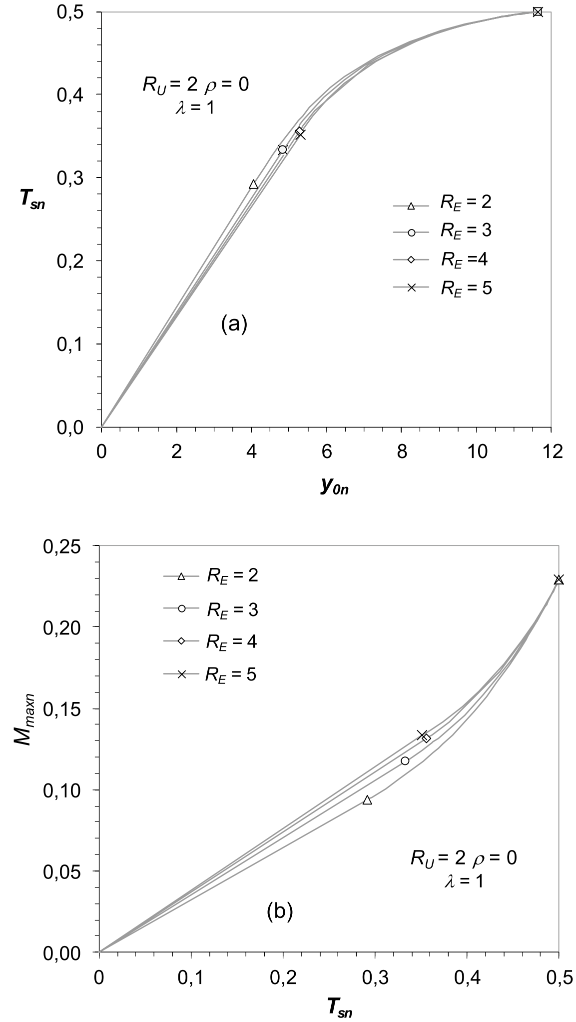

Fig. 14 Effect of R_E on the mobilization curve for $\lambda = 1$ $R_U = 2$ and $\rho = 0$: **a** T_{sn} *vs* y_{0n} **b** M_{maxn} *vs* T_{sn}

head deflection y_{0n} and maximum bending moment M_{maxn} calculated for some intermediate values of the normalized shear force ($T_{sn} < 0.5$) for different combinations of λ, R_E, R_U and ρ. As expected, for increasing values of the embedment ratio λ, y_{0n} decreases whereas M_{maxn} increases. At increasing λ the effect of R_E and R_U tends to be negligible.

Finally, it can be observed that the effect of ρ is slightly appreciable only for the lower investigated values of λ and R_U and for high value of T_{sn} when soil plasticization occurs also below the sliding surface (see Fig. 3c, d, e); otherwise, when soil plasticization occurs only above the sliding surface (Fig. 3a) the values of y_{0n} and M_{maxn} obtained for $\rho = 1$ are perfectly coincident with those obtained for $\rho = 0$. Therefore the values of y_{0n} and M_{maxn} calculated for $\rho = 1$ and $\lambda > 1.2$ are not included in Tables 7–8.

4.1 Effect of R_U

Tables 7, 8 and Figs. 11, 12 are obtained by assuming $R_E = R_U$. While the effect of R_U is null below the elastic threshold, it can be potentially appreciable in the elastic–plastic zone. As an example, Fig. 13 shows the curves T_{sn}-y_{0n} and M_{maxn}-T_{sn} for $\lambda = 1.2$, $R_E = 3$ and $\rho = 0$ at varying R_U. As expected, the curves are perfectly superimposed in the elastic range. Note that for $R_U > 1.68$ the elastic threshold is independent of

R_U, as the soil plasticization first occurs above the sliding surface and Eq. 32a—which does not include R_U—determines the beginning of the elastic–plastic part of the mobilization curve. For $R_U = 1.5$ the elastic threshold is slightly lower, as for this combination of R_E and R_U the elastic threshold is governed by the soil plasticization below the sliding surface (Eq. 32b). Only for T_{sn} greater than about 0.4 the curves are clearly distinct as the final values of y_{0n} and M_{maxn} depend on which plastic mode is reached (C1, C2 or C3) and this on turn depends on R_U and ρ. For λ = 1.2 mode C3 always develops when $R_U > 2.36$ and the final values of y_{0n} and M_{maxn} become independent of R_U. This implies that the mobilization curve relevant to R_U = 3—or in general for $R_U > 2.37$—is perfectly coincident with that for $R_U = 2.37$.

4.2 Effect of R_E

Figure 14 shows different mobilization curves T_{sn}-y_{0n} and M_{maxn}-T_{sn} obtained by varying R_E for an assigned combination of λ, $/R_U$ and ρ (λ =1; R_U = 2; ρ = 0). In this case the final values of y_{0n} and M_{maxn} are the same, as they depend only on R_U and ρ. The elastic thresholds and the extent of the elastic–plastic zone depends on R_E. For a given value of T_{sn} (<0.5) both y_{0n} and M_{maxn} slightly increase with R_E. The effect of R_E becomes negligible approaching the plastic condition.

5 Numerical Example

The procedure for designing a stabilizing pile is illustrated by a numerical example.

The soil profile includes an unstable cohesionless layer (γ = 18 kN/m^3; ϕ = 30°; n = 2000 kN/m^3) of thickness 3.75 m overlying a stable layer of OC clay. Let us assume that a traditional two-dimensional stability analysis requires an additional resistant force of 245 kN/m to achieve the desired safety factor.

Consider a row of stabilizing bored concrete piles (E_p = 32 GPa) with D = 1.5 m and L = 8.4 m, so that the condition of rigidity of Eq. (7) is satisfied. Moreover consider a center to center spacing of 6 m (i.e. 4D), which implies that each pile must support 1470 kN. For this spacing it is reasonable to calculate the value of m_1 using the relationship suggested by Fleming et al. (2009) for isolated piles in sand, i.e. $m_1 = DK_P^2\,\gamma$ = 243 kN/m^2. Assuming for the stable layer the lateral resistance per unit length, $P_{u2,}$ equal to 1950 kN/m and subgrade modulus E_{s2} = 20 MPa, the dimensionless parameters T_{snR}, λ, R_E, R_U and ρ can be computed as 0.43, 1.24, 2.67, 2.14 and 0, respectively.

With this input the normalized shear force at the elastic threshold T_{sne} is computed as 0.37; then, for the required resistant force, the pile response falls in the elastic–plastic range.

Using the values of Table 7 a first linear interpolation is made to compute y_{0n} for λ = 1.24 and R_U = 2, obtaining 3.966 and 4.582 for T_{sn} = 0.40 and T_{sn} = 0.45, respectively. Repeating the interpolation for R_U = 3 gives y_{0n} = 4.026 for T_{sn} = 0.40 and y_{0n} = 4.602 for T_{sn} = 0.45.

Starting from these values, a second interpolation is performed to calculate the values of y_{0n} relevant to T_{sn} = 0.43 which are equal to 4.3356 for R_U = 2 and 4.3716 for R_U = 3. Finally, a third linear interpolation is required to compute the value of y_{0n} for R_U = 2.14 obtaining y_{0n} = 4.34, which corresponds to y_0 =4.34• $m_1/(nR_E)$ = 19.8 cm.

The same procedure can be applied to evaluate the maximum bending moment by the data of Table 8. Specifically, by triple linear interpolation a value of M_{maxn} = 0.1817 is obtained, i.e. M_{max} = 0.1817•$m_1L_1^3$ = 2328 kNm.

The pile head deflection and the maximum bending moment are 82% and 79%, respectively, of those calculated at the plastic threshold using the closed-form equations of case C2 listed in Table 5 which gives y_{0n} = 5.284 and M_{maxn} = 0.2295.

Note that the previous elastic–plastic computations are strictly valid for R_E = R_U = 2.14; by performing a specific numerical analysis with R_E = 2.67 and R_U = 2.14 the normalized pile head deflection and the maximum bending moment are computed as 4.325 and 0.1797, with a difference percentage of about 1% in comparison with the values obtained by the simplified procedure based on Tables 7, 8.

6 Conclusions

An approach based on the modulus of subgrade reaction has been proposed to analyze the response of a rigid unrestrained passive pile subjected to a uniform horizontal soil movement in two-layered soil. The investigated soil profile includes an unstable layer with the modulus of subgrade reaction and the ultimate strength that vary linearly with depth, whereas both are assumed to be constant in the stable layer. In the investigated soil profile the ultimate strength vary linearly with depth in both unstable and stable layer, and the modulus of subgrade reaction is assumed to increase with depth in the unstable layer, whereas is assumed to be constant in the stable layer.

Using dimensionless parameters, the pile response has been analyzed in terms of the shear force developed at the sliding surface, maximum bending moment and pile head deflection.

Unlike some previous studies, the analysis has been focused not only to the soil ultimate state but also to the intermediate soil response, when soil reaction is fully elastic or locally plastic along the pile shaft. The analysis described in this paper allows obtaining the mobilization curves, i.e. the relationships between soil movement, pile head deflection, maximum bending moment and shear force at the sliding depth. For the elastic part of the mobilization curves, analytical expressions have been derived to calculate internal forces, pile deformation and limiting soil movement beyond which the soil response ceases to be elastic. For usual pile embedment the extent of the elastic zone increases with the pile embedment (λ) and with the strength and modulus ratio at the layer interface (R_U and R_E) and in certain circumstances the pile response remains fully elastic until it reaches 90% of the maximum shear force at the sliding surface.

For the elastic–plastic part of the mobilization curves, a general case has been discussed and the governing equations have been also provided. In such a case the numerical solution of a nonlinear system is needed and closed-form solutions are not available. All the mobilization curves reach one of the possible three failure mechanisms already known in the literature (short pile, intermediate and flow mode). For the investigated soil profile, the occurrence of such failure modes is found to depend on the combined values of the embedment ratio (λ) and the strength ratio at the soil interface (R_U), as well as the ratio of the gradients of soil strength (ρ).

The results of a parametric study shows that the mobilization curves is strongly influenced by the embedment ratio (λ) while the effect of the soil properties (R_E, R_U and ρ) is minor.

Tabulated values of the normalized pile head deflection and maximum bending moment as a function of the required stabilizing force are provided for different combination of λ, R_E, R_U and ρ for a quick assessment of pile response. A simplified procedure has been described by a numerical example, to check the pile performance even in the elastic–plastic range without the need to solve the nonlinear system governing the problem. The accuracy of this design methodology was demonstrated to be very high, especially if compared with the intrinsic uncertainties involved in the choice of deformability and strength parameters of the soil layers.

Funding Open access funding provided by Università Politecnica delle Marche within the CRUI-CARE Agreement. The authors have not disclosed any funding.

Data Availability All data generated or analyzed in this study are included within the paper.

Declarations

Competing interests The authors have not disclosed any competing interests.

References

Ashour M, Ardalan H (2012) Analysis of pile stabilized slopes based on soil–pile interaction. Comput Geotech 39:85–97. https://doi.org/10.1016/j.compgeo.2011.09.001

Ausilio E, Conte E, Dente G (2001) Stability analysis of slopes reinforced with piles. Comput Geotech 28(8):591–611. https://doi.org/10.1016/S0266-352X(01)00013-1

Bellezza I, Caferri L (2018) Ultimate lateral resistance of passive piles in non-cohesive soils. Géotechnique Letters 8(1):5–12. https://doi.org/10.1680/jgele.17.00113

Bellezza I, Caferri L, Di Sante M, Fratalocchi E, Mazzieri F (2017) Elastic–plastic analysis of passive rigid piles in Cohesionless soils. Proc. XIX ICSMGE Seoul. (Lee

W, Lee JS, Kim HK, Kim DS eds). CRC Press. London (UK) and New York (NY). pp 2723–2726

Bellezza I (2020) Closed-form expressions for a rigid passive pile in a two-layer soil. Géotech Lett 10(2):242–249. https://doi.org/10.1680/jgele.19.00250

Cai F, Ugai K (2000) Numerical analysis of the stability of a slope reinforced with piles. Soils Found 40(1):73–84. https://doi.org/10.3208/sandf.40.73

Cai F, Ugai K (2003) Response of flexible piles under laterally linear movement of the sliding layer in landslides. Can Geotec Journ 40(1):46–53. https://doi.org/10.1139/t02-103

Cai F, Ugai K (2011) A subgrade reaction solution for piles to stabilise landslides. Géotechnique 61(2):143–151. https://doi.org/10.1680/geot.9.P.026

Chen LT, Poulos HG (1997) Piles subjected to lateral soil movements. J Geotech Geoenv 123(9):802–811. https://doi.org/10.1061/(ASCE)1090-0241(1997)123:9(802)

Chow YK (1996) Analysis of piles used for slope stabilization. Int J Numer Anal Methods Geomech 20(9):635–646. https://doi.org/10.1002/(SICI)1096-9853(199609)20:9%3C635::AID-NAG839%3E3.0.CO;2-X

De Beer EE, Carpentier R (1977) Discussion on the paper of Ito & Matsui (1975). Soil Found 16(1):68–82

Di Laora R, Maiorano RMS, Aversa S (2017) Ultimate lateral load of slope-stabilising piles. Géotech Lett 7(3):237–244. https://doi.org/10.1680/jgele.17.00038

Di Laora R, Fioravante V (2018) A method for designing the longitudinal spacing of slope-stabilising shafts. Acta Geotech 13(5):1141–1153. https://doi.org/10.1007/s11440-017-0617-2

Ellis EA, Durrani IK, Reddish DJ (2010) Numerical modelling of discrete pile rows for slope stability and generic guidance for design. Géotechnique 60(3):185–195. https://doi.org/10.1680/geot.7.00090

Fleming K, Weltman A, Randolph M, Elson K (2009) Piling Engineering, 3rd edn. Taylor & Francis, London (UK and New York (NY)

Fukuoka M (1977) The effect of horizontal loads on piles due to landslides. Proc. IX ICSMFE. Tokyo. 10th Spec Session, 27–42

Galli A, Maiorano RMS, di Prisco C, Aversa S (2017) Design of slope-stabilizing piles: from Ultimate Limit State approaches to displacement based methods. Riv Ital Di Geotec 51(3):77–93. https://doi.org/10.19199/2017.3.0557-1405.077

Georgiadis K, Sloan SW, Lyamin AV (2013) Undrained limiting lateral soil pressure on a row of piles. Comput Geotech 54:175–184. https://doi.org/10.1016/j.compgeo.2013.07.003

Guo WD (2014) Elastic models for nonlinear response of rigid passive piles. Int J Numer Anal Methods Geomech 38(18):1969–1989. https://doi.org/10.1002/nag.2292

Hassiotis S, Chameau JL, Gunaratne M (1997) Design method for stabilization of slopes with piles. J Geotech Geoenv Eng 123(4):314–323. https://doi.org/10.1061/(ASCE)1090-0241(1997)123:4(314)

Ito T, Matsui T (1975) Methods to estimate lateral force acting on stabilizing piles. Soils Found 15(4):43–59. https://doi.org/10.3208/sandf1972.15.4_43

Ito T, Matsui T, Hong WP (1979) Design method for the stability analysis of the slope with landing pier. Soils Found 19(4):43–57. https://doi.org/10.3208/sandf1972.19.4_43

Ito T, Matsui T, Hong WP (1981) Design method for stabilizing piles against landslide-one row of piles. Soils Found 21(1):21–37. https://doi.org/10.3208/sandf1972.21.21

Ito T, Matsui T, Hong WP (1982) Extended design method for multi-row stabilizing piles against landslide. Soils Found 22(1):1–13. https://doi.org/10.3208/sandf1972.22.1

Jeong S, Kim B, Won J, Lee J (2003) Uncoupled analysis of stabilizing piles in weathered slopes. Comput Geotech 30(8):671–682. https://doi.org/10.1016/j.compgeo.2003.07.002

Kanagasabai S, Smethurst JA, Powrie W (2011) Three-dimensional numerical modelling of discrete piles used to stabilize landslides. Can Geotech J 48: 1393–1411. https://doi.org/10.1139/t11-046

Kourkoulis R, Gelagoti F, Anastasopoulos I, Gazetas G (2011) Slope stabilizing piles and pile-groups: parametric study and design insights. J Geotech Geoenv Eng ASCE 137(7):663–677. https://doi.org/10.1061/(ASCE)GT.1943-5606.0000479

Kourkoulis R, Gelagoti F, Anastasopoulos I, Gazetas G (2012) Hybrid method for analysis and design of slope stabilizing piles. J Geotech Geoenv Eng ASCE 138(1):1–14. https://doi.org/10.1061/(ASCE)GT.1943-5606.0000546

Lee CY, Hull TS, Poulos HG (1995) Simplified pile-slope stability analysis. Comput Geotech 17(1):1–16. https://doi.org/10.1016/0266-352X(95)91300-S

Lei G, Su D, Cabrera MA (2022) Non-dimensional solutions for the stabilising piles in landslides in layered cohesive soils considering non-linear soil–pile interactions. Géotechnique 72(8):737–751. https://doi.org/10.1680/jgeot.20.P.267

Poulos HG (1995) Design of reinforcing piles to increase slope stability. Can Geotech J 32(5):808–818

Reese LC, Wang ST and Fouse JL (1992) Use of drilled shafts in stabilizing a Slope. In: Stability and performance of slopes and embankments–II. R.B. Seed and R.W. Boulanger eds. Geotechnical special publication 31(2), 1318–1332, ASCE New York (NY)

Smethrust JA, Powrie W (2007) Monitoring and analysis of the bending behaviour of discrete piles used to stabilize a railway embankment. Géotechnique 57(8):663–677. https://doi.org/10.1680/geot.2007.57.8.663

Sommer H (1977) Creeping slope in a stiff clay. Proc. IX ICSMFE. Tokyo. 10th Spec Session, pp 113–118

Terzaghi K (1955) Evalution of conefficients of subgrade reaction. Geotechnique 4:297–326

Viggiani C (1981) Ultimate lateral load on piles used to stabilize landslides. Proc. X ICSMFE. Stockholm, Vol 3, pp 555–560. ed. Committee of X ICSMFE. Balkema. Rotterdam. The Netherlands

Wei WB, Cheng YM (2009) Strength reduction analysis for slope reinforced with one row of piles. Comput Geotech 36(7):1176–1185. https://doi.org/10.1016/j.compgeo.2009.05.004

Won J, You K, Jeong S, Kim S (2005) Coupled effects in stability analysis of pile–slope systems. Comput Geotech 32(4):304–315. https://doi.org/10.1016/j.compgeo.2005.02.006

Yamin M, Liang RY (2010) Limiting equilibrium method for slope/drilled shaft system. Int J Numer Anal Methods Geomech 34(10):1063–1075

Zhang L (2009) Nonlinear analysis of laterally loaded rigid piles in cohesionless soil. Comput Geotech 36(5):718–724

Zhang L, Ahmari S (2013) Nonlinear analysis of laterally loaded rigid piles in cohesive soil. Int J Numer Anal Methods Geomech 37(2):201–220